RESEARCH ARTICLE

Macromolecular Bioscience
www.mbs-journal.de

Organic Functional Group on Carbon Nanotube Modulates the Maturation of SH-SY5Y Neuronal Models

Bahaa Daou, Alessandro Silvestri, Haizpea Lasa, Donato Mancino, Maurizio Prato, and Nuria Alegret**

Carbon nanotubes (CNT) have proven to be excellent substrates for neuronal cultures, showing high affinity and greatly boosting their synaptic functionality. Therefore, growing cells on CNT offers an opportunity to perform a large variety of neuropathology studies in vitro. To date, the interactions between neurons and chemical functional groups have not been studied extensively. To this end, multiwalled CNT (f-CNT) is functionalized with various functional groups, including sulfonic ($-SO_3H$), nitro ($-NO_2$), amino ($-NH_2$), and oxidized moieties. f-CNTs are spray-coated onto untreated glass substrates and are used as substrates for the incubation of neuroblastoma cells (SH-SY5Y). After 7 d, its effect is evaluated in terms of cell attachment, survival, growth, and spontaneous differentiation. Cell viability assays show quite increased proliferation on various f-CNT substrates (CNTs-NO_2 > ox-CNTs ≈ CNTs-SO_3H > CNTs ≈ CNTs-NH_2). Additionally, SH-SY5Y cells show selectively better differentiation and maturation with $-SO_3H$ substrates, where an increased expression of β-III tubulin is seen. In all cases, intricate cell-CNT networks are observed and the morphology of the cells adopts longer and thinner cellular processes, suggesting that the type of functionalization may have an effect of the length and thickness. Finally, a possible correlation is determined between conductivity of f-CNTs and cell-processes lengths.

1. Introduction

In neurotraumatic injuries or neurodegeneration diseases, a fibrotic tissue is formed in addition to scarring, which, in turn, hampers the electrical neuronal communication.[1] The poor spontaneous regeneration ability of neurons, together with the lack of efficacious treatments available, make these kinds of diseases lethal, and significantly reduces the life expectancy of the patients.[2] For this reason, the past decade has seen a raising on neural tissue engineering and regeneration, pointed as the potential solution to find a cure.[3] The core of tissue engineering is to find suitable materials able to provide excellent interaction and support for cells. Various cell lines have been used to help get new insights on neurological processes and regeneration through neuronal models.[4–7] Among the most common ones, neuroblastoma cells (SH-SY5Y) can be easily differentiated into mature neurons upon neurotoxic treatments and, thus, widely used as models for neurodegenerative disorders.[8]

To design neuro-promoting substrates and understand their effect on neuronal networks, the synaptic processes is key for neuronal cell growth, maturation, and proper functions.[9,10] Furthermore, materials with electrical properties demonstrated to promote the synaptic function of neurons and greatly enhance the formation of neuronal networks.[11,12] Among them, carbon nanotubes (CNT) have become the leading edge of nanotechnology applied in neuroscience and widely used as 2D substrates to study neuronal cell models.[13–17] Yet in the firsts articles, CNTs demonstrated to promote neuronal maturation, growth, proliferation, and boost the synaptic signaling.[18] More recently, we have proved that CNT can differentiate SH-SY5Y cells without pre-exposing the cells to a differentiation medium.[19,20] Similar observations were found in different types of stem cell lines.[19,21–24]

In common cell cultures, cells interact with the substrates through various mechanisms: protein adhesion, ionic interaction through multiple coatings, and integrin binding.[25] From a chemical point of view these are molecular interactions that can be governed mostly by organic functional groups.[26] To this end, CNTs can be functionalized with various moieties to make them either more biocompatible,[27] dispersible or more hydrophilic,[24,28] which is an interesting asset to promote

B. Daou, A. Silvestri, H. Lasa, D. Mancino, M. Prato, N. Alegret
Center for Cooperative Research in Biomaterials (CIC BiomaGUNE)
Basque Research and Technology Alliance (BRTA)
Donostia-San Sebastián 20014, Spain
E-mail: mprato@cicbiomagune.es; nalegret@cicbiomagune.es
B. Daou, H. Lasa
Neuromuscular Diseases Group, Neurosciences Area
Biodonostia Health Research Institute
Donostia/San Sebastián 20014, Spain
M. Prato
Ikerbasque
Basque Foundation for Science
Bilbao 48013, Spain
M. Prato
Department of Chemical and Pharmaceutical Sciences
Universitá Degli Studi di Trieste
Trieste 34127, Italy

The ORCID identification number(s) for the author(s) of this article can be found under https://doi.org/10.1002/mabi.202300173

DOI: 10.1002/mabi.202300173

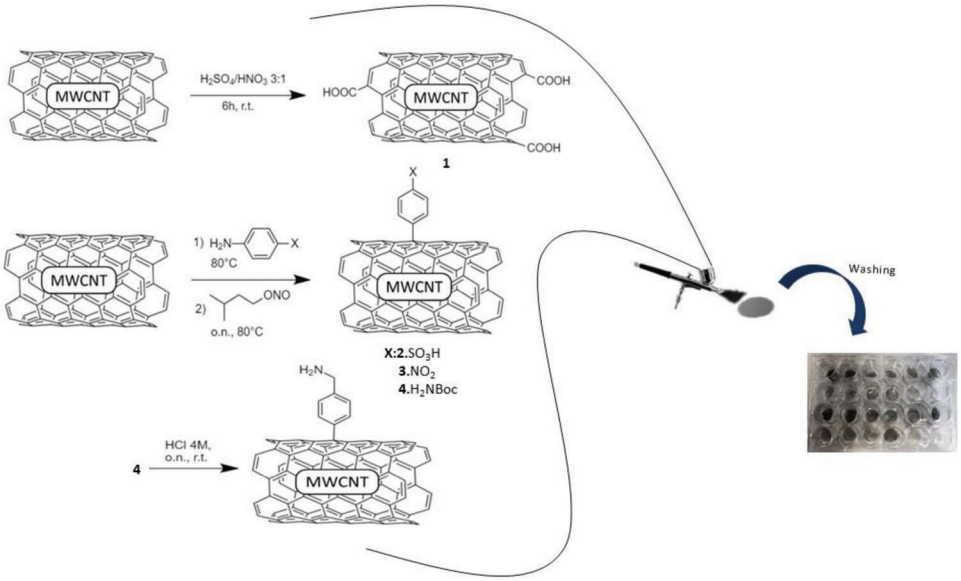

Figure 1. Summary of the various CNTs functionalization strategies and the preparation of f-CNT substrates by spray coating.

cell-CNT interaction.[19,29] In particular, previous works using functionalized CNT showed great capabilities of these structures in neural differentiation and proliferation. Shao et al. studied carboxylated CNTs (COOH-CNT) and pristine CNT/Polydopamine (PDA) substrates via layer-by-layer assembly with poly(dimethyldiallylammonium chloride) (PDDA).[30] Their results showed that CNT enhanced maturation in neural stem cells (NSC), suggesting that the interaction between CNT and NSC was mediated by integrins. More importantly, CNTs activated focal adhesion kinase (FAK), which in turn upregulated cellular adhesion, proliferation, and maturation. However, in this study no preference is shown to the functional moiety of the CNT. A similar study in 2004 evaluated the effect of functionalized CNT-COOH, CNT-poly-m-aminobenzene sulfonic acid (PABS), and CNT-ethylenediamine with hippocampal neurons.[31] The results suggested a dependence of neurite outgrowth on the CNT charges: the amine-terminated CNT showed highest neurite length, whereas sulfonic-terminated CNT showed more neuronal branching.

CNTs also gained much attention with in vivo studies. In one done on the spinal cord, CNTs were found to restore neural signal in severed spinal cord in mice, as well as significant recovery and functionality. CNT-based scaffolds were also able to support angiogenesis, which is crucial for regeneration.[32,33] In another example, Hu et al. used amine functionalized CNTs encapsulated with polycaprolactone (PCL) and gelatin to create conductive nanofibers that, combined with bone-marrow derived mesenchymal stem cells, were as nerve guidance conduit (NGC) for sciatic nerve regeneration.[34] Interestingly, over 40% myelination ratio in CNT-based NGC was seen, twice that of the control. Finally, Pi et al. used a solvent-drying method to produce PCL-based 3D scaffolds with COOH functionalized CNTs, which showed significantly enhanced regeneration compared to PCL CNT-free conduits.[35] These findings emphasize the importance of CNT-based conductive scaffolds in promoting neural regeneration.

Herein, we aim to evaluate how various functional groups present on f-CNT affect cellular attachment, spontaneous differentiation, and maturation of the neuroblastoma SH-SY5Y cells. To the best of our knowledge, there is little reported literature contribution studying the effect of functional groups in cell growth or spontaneous differentiation. To this end, we have used oxidized CNT (oxCNT) to obtain oxygen-bearing moieties which will render the nanotube more hydrophilic. In addition, taking advantage of the Tour reaction, we have introduced diverse functional groups on the CNTs' surfaces, including sulfonic acid (–SO_3H), nitro group (–NO_2), and amino group (–NH_2). The f-CNTs composition and electrochemical properties has been fully characterized. Air-sprayed f-CNT coatings prepared on glass were then used as substrates to incubate neuroblastoma SH-SY5Y cells and assess their viability and maturation to evaluate the effect of the different functional groups.

2. Results and Discussion

2.1. f-CNT Synthesis and Characterization

The CNTs were functionalized with four different functional groups using previously described synthetic strategies shown in **Figure 1**. On one hand, CNTs were oxidized via acidic treatment obtaining CNT bearing COOH-groups among others.[36] On the other, the Tour reaction was used to introduce 4-phenylsulfonic acid, 4-nitrophenyl, and 4(amino methyl)phenyl groups.[37]

Figure 2a summarizes the elemental composition of various CNTs obtained through X-ray Photoelectron Spectroscopy (XPS) analysis, which confirms the successful functionalization of all f-CNTs. As expected, ox-CNTs show an increase in oxygen content (9.82%), compared to p-CNTs (1.98%), due to the various oxy-functional moieties introduced by the acidic treatment. This is further confirmed by the high-resolution spectrum of the C 1s core, showing a significant increase in C—O, C═O, and O—C═O compared to those of p-CNTs (Figures S1 and S2, Supporting

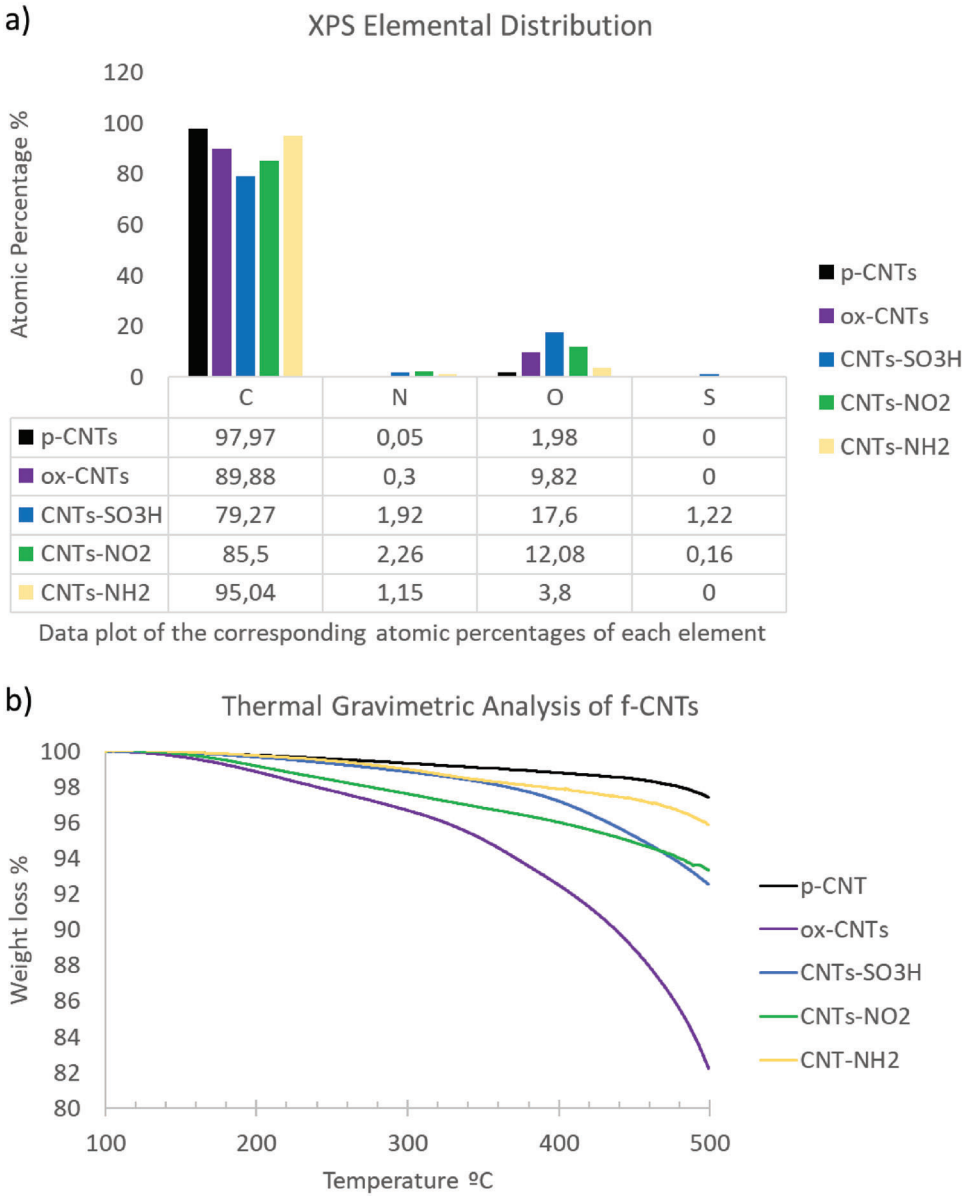

	C	N	O	S
p-CNTs	97,97	0,05	1,98	0
ox-CNTs	89,88	0,3	9,82	0
CNTs-SO3H	79,27	1,92	17,6	1,22
CNTs-NO2	85,5	2,26	12,08	0,16
CNTs-NH2	95,04	1,15	3,8	0

Data plot of the corresponding atomic percentages of each element

Figure 2. a) XPS Elemental composition (the data values are expressed in atomic percentages and reported in the table) of the functionalized CNTs, b) The weight loss at 500 °C obtained by TGA allows the calculation of the CNTs functionalization degrees (FDs).

Information).[39] Similarly, in the case of CNTs-SO_3H, an evident increase in sulfur content to 1.22% and oxygen content to 17.60% can be attributed to the addition of the sulfonic group. The high-resolution spectrum (Figure S3, Supporting Information) of S 2p core confirms the presence of sulfonic acid, as indicated by the peak centered at 168 eV, attributable to S–O bonds.[40] For CNT_S-NO_2, N, and O contents increase to 2.26% and 12.08%, respectively. The high- resolution spectrum of the N 1s core shows a major component at around 406 eV, which can be attributed to NO_2 groups (Figure S4, Supporting Information).[41] Finally, for CNTs-NH_2 an increase of N content to 1.15% compared to p-CNTs is attributed to the addition of amino group, an increase of O content to 3,8 can be due to increased oxy-bearing moieties during functionalization. High-resolution nitrogen spectrum CNTs-NH_2 (Figure S5, Supporting Information) shows a one component peak at around 400 eV which can be attributed to NH_2 groups.[41]

The analysis of the nitrogen content in the CNTs can be affected by the presence of nitrogen bearing sub-products of the Tour reaction, as testified by the elemental composition reported in Figure 2. Therefore, thermogravimetric analyses (TGA) was used to confirm the functionalization of the CNTs and quantify the functionalization degree. TGA measurements (Figure 2b) were performed under inert atmosphere to better distinguish between the degradation of the CNT and the organic moieties. In this sense, 500 °C was taken as the reference temperature because the decomposition of CNTs under such conditions can be considered negligible. At first glance, all TGA curves show that

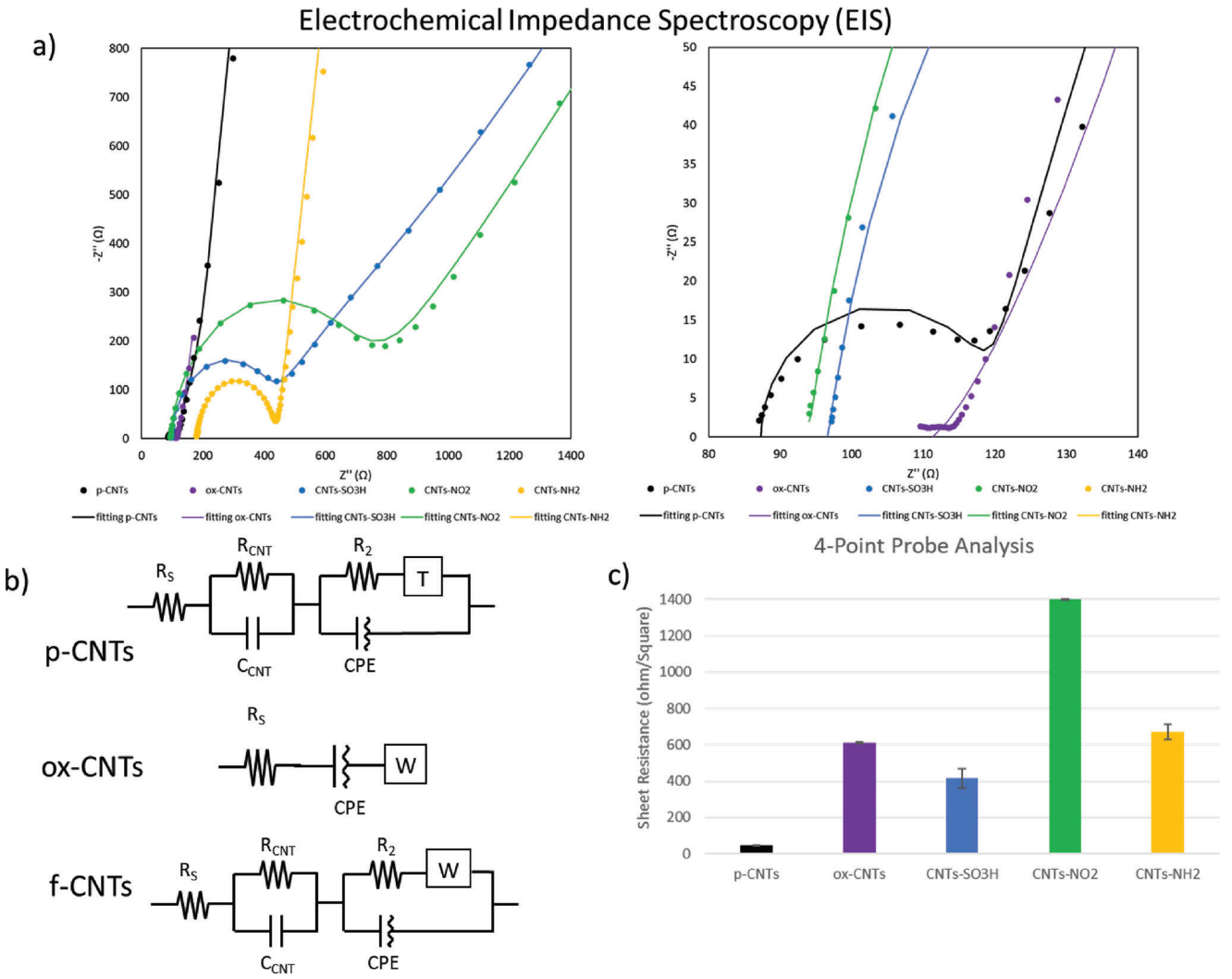

Figure 3. a) Electrochemical Impedance spectroscopy (EIS) performed in 100×10^{-3} M PBS buffer (containing 100×10^{-3} M KCl, pH 7.4) at a potential of 0 V (vs REF), with a perturbation of 10 mV and in a frequency range comprised between 1 MHz and 10 mHz, b) with the corresponding circuits used for fitting the data. Additionally, c) 4-Point Probe analysis gave new insights on the conductivity of these CNT substrates.

the temperature degradation proceeds in a similar manner for all f-CNT. FDs are calculated by subtracting the weight loss percentage of f-CNTs from p-CNT_S. The achieved functionalization degree is in accordance with previously reported works.[38] ox-CNTs showed a functionalization degree of around 14.838%, while the functionalization degrees of the reactions with diazonium salts were as follows: 5.6% for CNTs-SO_3H, 4.25% CNTs-NO_2, and 2% for CNTs-NH_2. The lower functionalization degree of NH_2 can be explained by the deprotection step to which these nanotubes undergo after the Tour reaction.

The electrical properties of pristine, and functionalized CNTs were investigated through EIS, seeking a relation with the biological response in contact with neuroblastoma cell line **Figure 3** and Figure S6 in the Supporting Information). With this aim, two main variables have been analysed: the resistance at the charge transfer through CNTs/electrolyte interface (R_{CT}) and the capacitive behaviour related to the formation of a charge double layer at the interface (C_{CNT}) (**Table 1**). p-CNTs present an impedance spectrum like the ones previously reported for this material Figure 3a.[42] At high frequencies (below 100 kHz) the resistive behaviour predominates as indicated by the phase angle close to 0° and the constant impedance in the bode plot Figure S6a in the Supporting Information. The value of the impedance at high frequencies represents the uncompensated resistance (R_S) of the electrolyte, electrode, and cables (Table 1). At higher frequencies (between 100 kHz and 100 Hz) a Rendall circuit is present, which represents the resistance of the CNTs at the charge transfer. In

Table 1. Summary of the EIS values of p-CNTs and f-CNTs.

	p-CNTs	ox-CNTs	CNTs-SO_3H	CNTs-NO_2	CNTs-NH_2
R_s [Ω]	86,53	108,3	93,45	91,29	180,38
R_{CT} [Ω]	36,58	N/A	373,6	734	256,76
C_{CNT}	2,34 μF	9,1 mF	4,51 μF	3,51 μF	8,8 μF

the Nyquist plot, the Rendall circuit is characterized by a characteristic semicircle shape, whose diameter correspond to the R_{CT} value of the material. The reduced diameter of the semicircle indicates a low charge transfer resistance (R_{CT} = 37.33 Ω) as expected from this material. At lower frequencies a capacitive behaviour predominates as indicated in the Bode plot by the phase angle which is closer to 90°. This capacitive behaviour, characteristic of CNTs, is represented in the Nyquist plot by a vertical tail at decreasing frequencies (Figure 3a).[42,43] To achieve the best fitting of the EIS data, an element describing the diffusion regime of ions toward the electrode surface must be considered. The equivalent circuits used to fit the EIS data are reported in Figure 3b and are in accordance with circuits previously reported in literature for CNTs.[42,44–46] The chemical modification of the CNTs induces a drastic change in the impedance spectra of the materials. Ox-CNTs shows a fully capacitive behaviour, and no charge transfer resistance can be highlighted from the spectrum. As result, the electrical equivalent circuit used to fit these data is comprised of R_s, a constant phase element (CPE) and a Warburg diffusion (W), which was inserted to model the diffusion of ions close to the surface. These experimental finding is in accordance with the fact that the Ox-CNTs are enriched of negatively charged groups which contributes to accumulating more cations on the surface and therefore creating a consistent double layer of charges. The CNTs functionalized by mean of the Tour reactions instead present a more pronounced resistance to charge transfer, when compared to p-CNTs, indicating that the radical reaction introduces defects in the Sp^2 conjugated structure of the CNTs. In fact, the charge transfer resistance of the CNTs-NH_2, CNTs-SO_3H, CNTs-NO_2 increases accordingly with the functionalization degrees saw through TGA. Regarding the capacitive behaviour, CNTs-SO_3H, CNTs-NO_2 shows a similar capacitance value to p-CNTs, while the positively charged CNTs-NH_2 shows slightly higher one (8.8 μF). The values of the uncompensated resistance (R_S), charge transfer resistance (R_{CT}), and capacitance of each material are reported in Table 1.

Finally, 4PP analysis allows the measurement of various sheet resistance of the prepared substrates Figure 3c. P-CNTs showed lowest sheet resistance (highest conductivity). The sheet resistance increased upon functionalization with highest sheet resistance seen with CNTs-NO_2

2.2. In Vitro Analysis

The prepared f-CNT substrates were used as substrates for in vitro analysis with neuroblastoma SH-SY5Y cells. SH-SY5Y cells are highly adherent, as they rely on protein adhesion directly onto treated polystyrene flask, proliferative and commonly utilized as models upon differentiation as they provide insights into the behavior of mature neurons.[25] In particular their maturity and differentiation can be assessed by observing their morphology, β-III tubulin, cell process length, and viability. The effects materials produced on this model can be extrapolated to mature neurons in a more cost-effective and time-efficient manner. Upon incubation onto f-CNT substrates, all cells survived for the whole duration of the experiment (7 d), as confirmed with the viability analyses plotted in **Figure 4**a and the optical images at day 3 and day 7 shown in Figures S7 and S8 in the Supporting Information, respectively. Neuroblastoma cells presented higher viability rates and preference when cultured on ox-CNTs, CNTs-SO_3H, and CNTs-NO_2 compared to the 2D control by around 22%, 20%, and 35%, respectively.

Spontaneous differentiation and, therefore, maturation were also evaluated. We incubated the cells for a period of 7 d and studied the increased rate of differentiation via β-III tubulin staining and quantification, which is a marker expressed mainly in neurons and associated with neurogenesis, maturation, and axon guidance. β-III tubulin/Actin ratio for each sample was calculated by measuring the fluorescence of β-III tubulin and Actin (Epifluorescence microscopy) and calculating the intensity of each marker. As shown in Figure 4b, SH-SY5Y cells in presence of CNT showed higher expression of β-III tubulin in all f-CNT substrates compared to the control. Among them, CNTs-SO_3H substrates showed the highest expression of tubulin, followed by CNTs-NH_2, CNTs-NO_2, and ox-CNTs.

Furthermore, cells on f-CNT substrates showed longer cellular processes compared to the control (Figure 4c). This can significantly stand out in CNTs-SO_3H, CNTs-NH_2, and p-CNT with cellular processes lengths of 52 ± 19, 46 ± 17.3, and 45 ± 10 μm respectively, which is in agreement with previous publications.[31] On the other side, we found no direct correlation between neurite-like lengths and tubulin quantification or total cell number.

Using differential interference contrast (DIC), the distribution and morphology of cells along the substrate was studied. In general, higher cell densities were observed on large CNT aggregations regardless the functionalization or surface chemistry of those substrates. To further understand the results obtained, we have examined the networks formed by the cells showed in **Figure 5**. In addition, we observed that the saturation of β-III tubulin fluorescence is highest when cells interact with the CNT aggregation highlighted by the arrows on Figure 5, and a similar elevated expression was observed in f-CNT aggregation with filamentous-actin due to the formation of a Cell-CNT-Cell network.

Furthermore, neuroblastoma cells appear to attach both f-CNT and p-CNT aggregation growing axons-like in an intrecate manner (arrows in Figure 5 and zoomed images in Figure S9 in the Supporting Information), hence suggesting the dependance on CNTs for the axons elongation of the cells, a behaviour usually attributed to glial cells´ effect on mature neurons. For instance, as shown in Figure S10 (Supporting Information), in the case of CNTs-NO_2, which present a significantly higher resistivity and, thus, lower conductivity, we can notice a decrease in axon-like lengths. In comparison, most CNT substrates (pristine-CNTs, CNTs-SO_3H, and CNTs-NH_2), which are more conductive than 2D control rather show a significant increase in axon-like length, suggesting the importance of conductivity in aiding cellular processes length. In all the other materials, the growth of cell processes was impulsed by higher conductivity of the f-CNTs. However, no correlation between capacitive nor the conductive behaviour of the CNTs and cell maturation (as indicated by β-III tubulin quantification) was observed. For example, CNTs-SO_3H showing the highest β-III tubulin expression is neither the most conductive nor the most capacitive. Hu et al. suggested that the neurite growth on carboxylated multi-walled carbon nanotubes

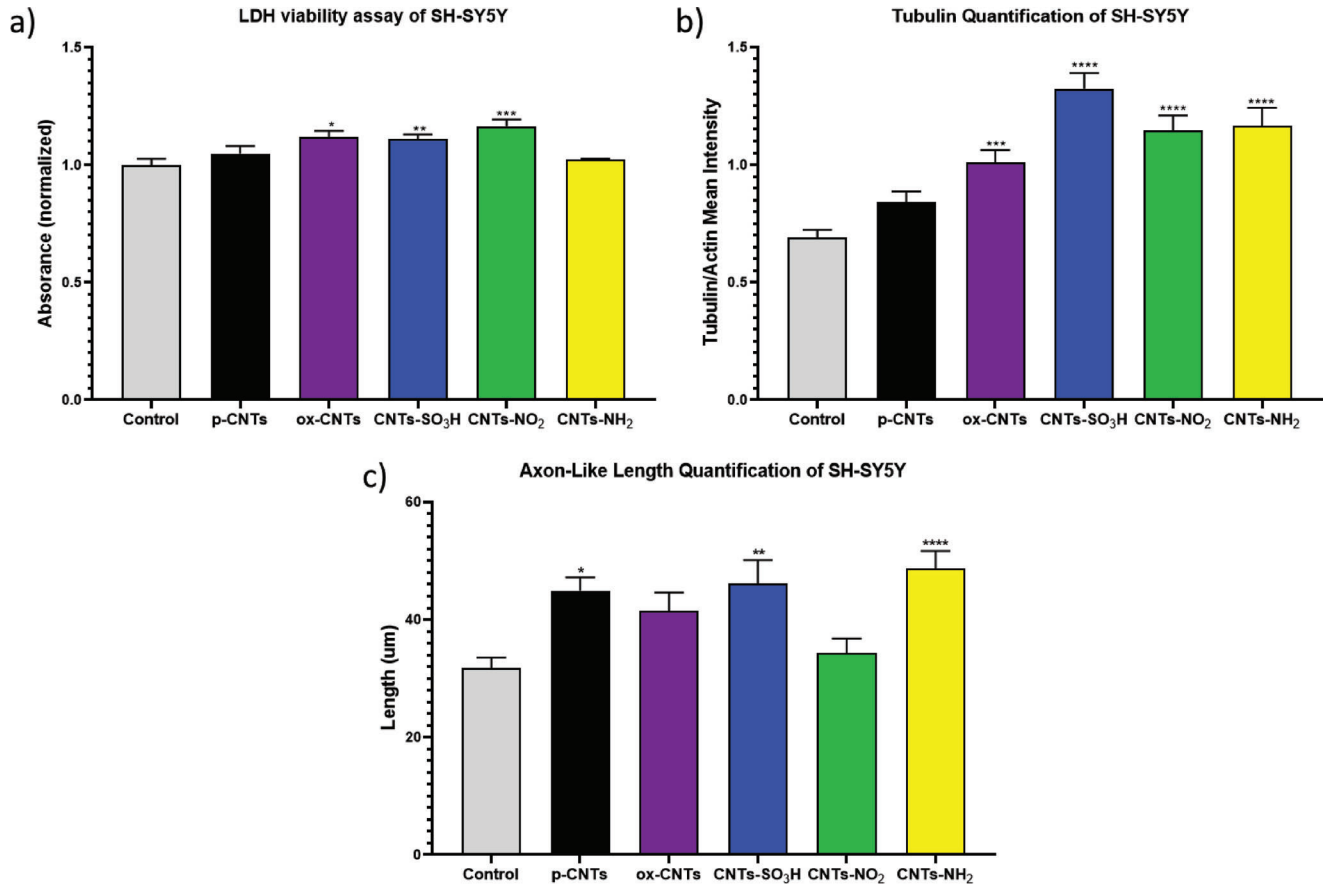

Figure 4. In vitro analysis of SH-SY5Y cell line incubated onto f-CNT coverslips for 7 d. a) Lactate dehydrogenise (LDH) assay done using the supernatant of each well after 7 d allows us to measure the viability of SHSY5Y cells. b) Quantification of tubulin/actin obtained from epifluorescence microscopy (n = 96 cells). c) Axon-like lengths calculated from epifluorescence microscopy (n = 96 cells). Values are considered statistically significant if ($P < 0.05$).

(MWCNT-COOH) (p*K*a COOH group ≈4.5, deprotonated), MWCNT- ethylenediamine (p*K*a NH_2 group 9.9), and MWCNT-poly-m-aminobenzene sulfonic acid (zwitterionic/neutral) substrates depend on the surface charges.[47] Our results are in agreement with this claim, since CNTs-SO_3H prepared from 4-amino sulfanilic acid (p*K*a ≈3.2, deprotonated in cell media, pH = 8) is the most charged. Nonetheless, another possible indication to this preferential expression could be the fact that more H-bonding sites were available for cells to attach even more strongly onto the f-CNTs and this could also explain why a significant increase in β-III tubulin expression is seen in all the other f-CNTs.

3. Conclusions

With the increase of CNT-based biofunctional materials for neural applications, the need to understand basic interaction between neuronal cells and CNT from one side and neuronal cells and functional groups on the other is essential. We have demonstrated that upon incubating neuroblastoma cells with functionalized CNTs, an elevated viability is observed. More interestingly, SH-SY5Y after 7 d of incubation spontaneously differentiated and matured as proven by the increase in β-III tubulin expression, showing preference towards all f-CNTs, and more prominently to CNTs-SO_3H. Additionally, neuroblastoma cells grown on CNT substrates showed longer and thinner cellular processes, which further reaffirm the positive effect of CNT on cell integrity. Finally, neuronal networks were shown to be selective towards CNT aggregations (mostly seen on CNTs-SO_3H), forming intricate structures of CNT-cell networks. We suggest that CNT can have a similar behaviour in acting as glial cells. Additionally, surface charges and hydrogen bonding sites seem to play an important role in cell processes development and length, thus in cell maturation. Our results lay grounds for the use of real-to-in-vivo 3D functionalized CNT-based scaffolds for tissue engineering and neural regeneration, directing through functional moieties, cell proliferation, maturation, and differentiation in a 3D network.

4. Experimental Section

Materials: Carbon nanotubes (CNT, >95%) were purchased from Nanoamor Inc. (stock# 1237YJS: inner diameter, 5–10 nm; outside diameter, 20–30 nm; length, 0.5–2 μm) and further purified with concentrated HCL for 6 h in a sonication bath. Isoamyl nitrite, anilines (sulfanilic acid, 4-nitroaniline, 4-[(*N*-Boc)aminomethyl]aniline)), and indium tin oxide coated PET (ITO) sheets were purchased from Sigma Aldrich. The solvents were acquired from Carlo Erba Reagents SAS, Sabadell, Spain. All reagents and solvents were used as received with no further purification.

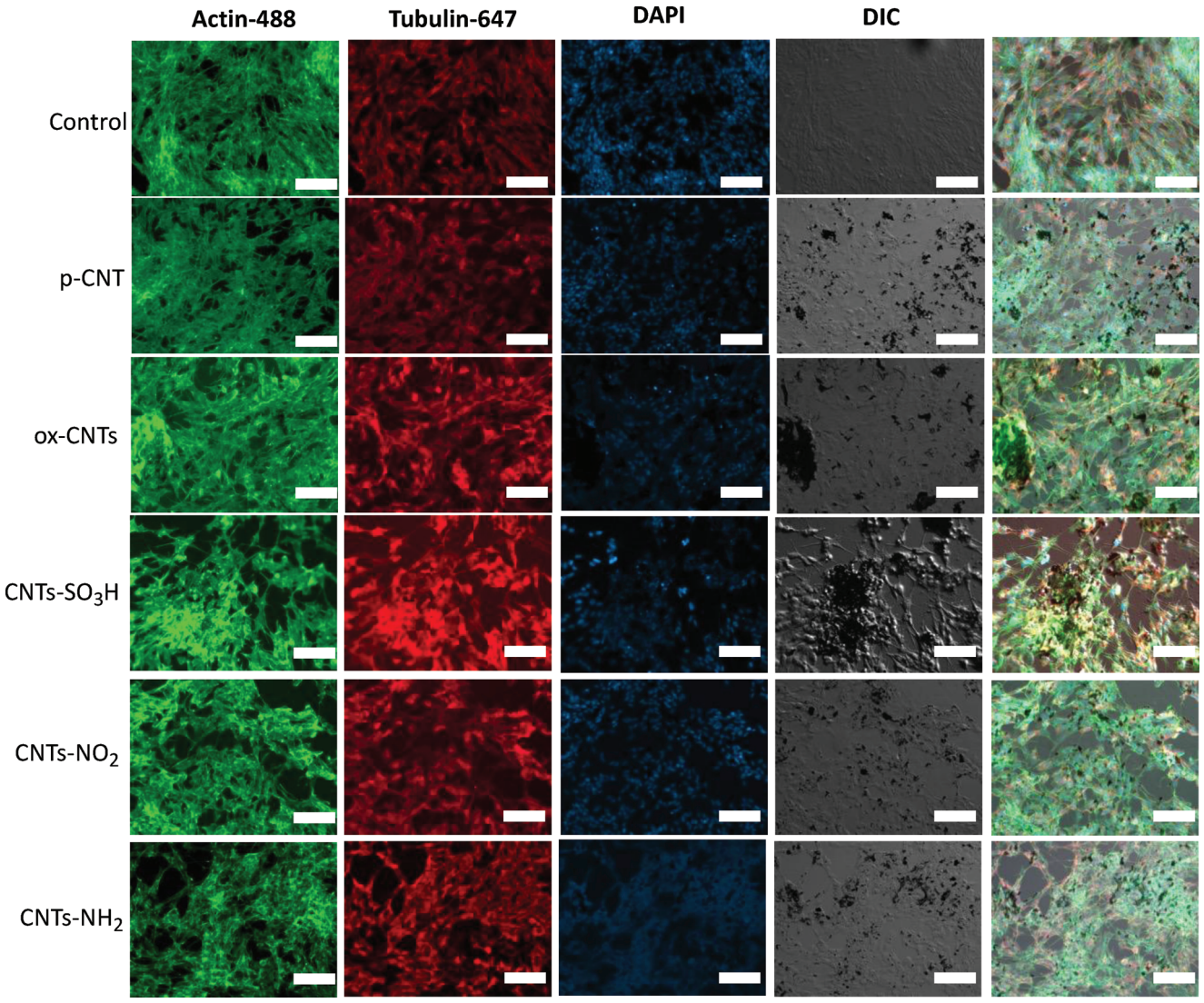

Figure 5. Epifluorescence images of f-CNT substrates with SH-SY5Y cells after 7 d incubation. Scale bar: 100 µm.

Neuronal SH-SY5Y cell line was purchased from ATCC-LGC and cultured in Dulbecco's ´Modified Eagle Medium (DMEM, GIBCO) premixed with Nutrient Mix F12 Ham media (1:1 ratio), containing 2×10^{-3} M L-glutamine (Gibco), 100 U mL^{-1} penicillin, 100 µg mL^{-1} streptomycin (Gibco), 0.5×10^{-3} M sodium pyruvate and 10% heat-inactivated fetal bovine serum (Gibco). The PBS buffer was purchased in tablets and prepared following manufacturer procedures (Sigma-Aldrich), corresponding to 10×10^{-3} M phosphate buffer containing 137×10^{-3} M NaCl and 2.7×10^{-3} M KCl at pH 7.3

CNT Functionalization and Characterization: *Oxidation of CNT (ox-CNT, 1)*: Pristine CNT (p-CNT, 1 mg mL^{-1}) were dispersed in solution of concentrated H_2SO_3 and HNO_3 (3:1). The dispersion was then sonicated for 6 h, stirred overnight and diluted 1:10 in milliQ water. The ox-CNT were filtered over a PTFE membrane (45 µm) and rinsed with milliQ water until neutral pH was reached, then cleaned with diethyl ether, and finally dried under vacuum overnight.[36]

CNT Functionalization: Tour reaction procedures were adapted from ones previously reported in literature.[37,38] Briefly, pCNTs were dispersed in anhydrous DMF (1 mg mL^{-1}, 100 mL) using a sonication bath and the solution was purged with Ar for 15 min. Then, the corresponding aniline (3 mmol) was poured into each CNT dispersion. The anilines used were sulfanilic acid, 4-nitroaniline, and 4-[(N-Boc)aminomethyl]aniline to obtain the CNT-SO_3H, CNT-NO_2 and the CNT-NBoc functionalized products, respectively. After equilibration of the system at 80 °C, isoamyl nitrite (3.2 eq with respect the aniline) was added dropwise to the reaction mixture and left under stirring at 80 °C for 6 h. Afterwards, the suspension was filtered over a PTFE membrane (45 µm), and the solid redispersed and washed with DMF at least three times until a persistently colorless filtrate was obtained. Finally, CNTs were washed with Milli-Q water, and ethanol. Finally, the solid sample was rinsed with diethyl ether and left to dry at room temperature under vacuum.

To achieve the amine functionalization (CNTs-NH_2), the cleavage of the Boc protecting group was carried out by dispersing CNT-NBoc in aqueous HCl solution (4 M, 1 mg mL^{-1}) and left to stir overnight at room temperature. The product was filtered over a PTFE membrane (45 µm) and rinsed with Milli-Q water until neutral pH value is obtained, followed by rinsing with diethyl ether and dried under vacuum at room temperature.

Preparation of f-CNT-Coated Substrates: Circular glass coverslips (#1.5) suitable for cell culture and P96 plastic plates were air-sprayed with a solution of the desired f-MWCNT in a concentration of 1 mg mL^{-1} in water

using an airbrush. The coating was performed by 8 to 10 longitudinal passes over the glass coverslip warmed at 50 °C, to accelerate evaporation of the solvent and improve the homogeneity of the coating between passes.

Electrochemical Impedance Spectroscopy (EIS) Measurements: EIS measurements were performed in a three-electrode configuration using an electrochemical workstation Autolab MSTAT204 potentiostat/galvanostat (Metrohm). The working electrode (WE) was obtained by drop-casting 500 µL of water dispersion of f-CNTs (10 mg mL^{-1}) on ITO coated PET electrodes. The electrode area was confined by using a silicon circular mask with a diameter of 0.5 cm. Pt wire and Ag/AgCl electrodes were used as counter and reference electrodes, respectively. Measurements were performed in $100 \times 10^{-}$ м PBS buffer (containing $100 \times 10^{-}$ м KCl, Ph 7.4) at a potential of 0 V (vs REF), with a perturbation of 10 mV and in a frequency range comprised between 1 MHz and 10 mHz. The fitting of EIS data was performed using NOVA software v2.1.6 (Metrohm AutoLab B.V.).

4-Point Probe (4-PP) Measurements: 500 µL of a 10 mg mL^{-1} dispersion of MWCNT in water was drop-casted on glass substrates confining the solution to a circular shape of 0.5 cm of diameter using a circular silicon mask. The solvent was left to dry before measuring sheet resistance using Ossila 4PP machine (thickness ≈ 100 µm). The target current was set up in a range between 10 and 100 µA using 10 V as maximum voltage.

Thermal Gravimetric Analysis (TGA): TGA was performed under Nitrogen (25 mL min−1 flow rate) using a TGA Discovery (TA Instruments). The samples were equilibrated at 100 °C for 20 min and then heated at a rate of 10 °C min−1, in the range from 100 to 500 °C. Measurements of at least two repetitions were recorded and Trios V4.4.0.41128 (TA instruments) software was used to Analyze data and calculate. The corresponding functionalization degree (FD) was estimated from the TGA plots taken at 500 °C.

X-ray Photoelectron Spectroscopy (XPS): XPS measurements were carried out with 420 SPECS SAGE HR 100 system equipped with 100 mm mean radius PHOIBOS analyzer where 421 Mg Kα X-ray source was used. The measurements were carried out directly onto the f-CNT vacuum-dried powder. Fitting of XPS data was carried out using CasaXPS software.

In vitro Studies: *Cell Culture and Seeding*: SH-SY5Y cells were cultured in complete media (DMEM : F12, 10% heat-inactivated FBS, 1% l-glutamine, 1% streptomycin/penicillin, 0.5% sodium pyruvate, 0.5% nonessential amino acids) at 37 °C and 5% CO2 in tissue culture-treated 75 cm2-flasks (Nunc). For passaging, cells were detached from the flasks by incubation at 37 °C with trypsin-EDTA solution 1X (Sigma) and spun at 480 RCF for 5 min; the obtained pellet was resuspended in 1 mL of complete media. For cell counting, the cell suspension was diluted 1:2 in the exclusion dye Trypan Blue solution (Sigma) and 10 µL of the diluted cell suspension was counted with the automated cell counter (Countess, Invitrogen).

For immunostaining experiment, 1000 µL complete media containing 5×10^5 SH-SY5Y cells was added into the P24 wells containing the f-CNT coated coverslips and incubated for 7 d at 37 °C and 5% CO_2. For viability studies, 5000 SH-SY5Y cells were seeded onto P96 wells coated with functionalized CNT and incubated 7 d at 37 °C and 5% CO_2. All the substrates were UV-sterilized for 20 min before use.

Lactate dehydrogenise (LDH) Assay: The viability of cells grown was evaluated with the LDH CytoTox96 Non-Radioactive Cytotoxicity Assay kit (Promega). After culturing the cells for 7 d in f-CNT coated P96 wells, media was removed and 100 µL Lysis Solution 1× were added and the cells were incubated for 45 min at 37 °C and 5% CO2. For the LDH detection, 50 µL of each supernatant was transferred to empty wells and was mixed with 50 µL of substrate mix CytoTox96 Reagent and, after 30 min, the reaction was terminated by the addition of 50 µL of Stop Solution. Absorbance measurements were taken at 492 nm in a micro plate spectrophotometer (GeniosPro, Tecan).

All the collected data were represented as means of quadruplicates ±SD of 3 independent experiments ($n = 3$) and normalized to the average value of control wells. Student's t test was performed to draw statistical comparisons between two treatment groups. Differences were considered statistically significant at $p < 0.05$.

Immunocytochemistry: After 7 d of incubation, the f-CNT coated coverslips were washed once with PBS, fixed with 4% paraformaldehyde in PBS for 10 min, and washed again with PBS. Then cells were permeabilized and blocked with a solution containing 0.5% Triton X-100 and 2% bovine serum albumin in PBS 1× for 1 h at room temperature. The coverslips were incubated with anti-beta-III tubulin monoclonal antibody conjugated to Alexa Fluor 647 (1 µg mL−1 dilution, Abcam) in blocking solution as diluent at 4 °C overnight in the dark. Then, fixed cells were washed 3 times with PBS 1× and incubated with Actin Green 488 Ready Probes Reagent (1:10 dilution, Invitrogen) for 30 min in the dark. Nuclei were stained for 1 h with 50 × 10−9 m 2-(4-amidinophenyl)−1H -indole-6-carboxamidine (DAPI) in PBS. Coverslips were mounted with Prolong Diamond Antifade (Invitrogen) before imaging.

Epifluorescence Imaging and Differential Interference Contrast (DIC) Microscopy Imaging: Images were taken in a laser scanning microscope (lsm880 AxioObserver, Zeiss) employing excitation at 633 nm. ZEN software was employed to process taken images including DIC. Single dual-channel images of 1 µm optical section at higher magnifications using the Plan-Apochromat 63×/1.40 Oil DIC M27 objective were collected.

For the **quantification** of β-III tubulin and actin stain, fluorescent images were analyzed using ImageJ program (National Institutes of Health, USA). In the analysis, regions of interest (ROIs) were selected in the cytoplasm. The fluorescent intensity of the pixels localized in the cytoplasm was averaged for each condition after removing the background signal (the fluorescent intensity of the pixels localized in areas outside the cells in each image). Results are expressed as a ratio between – β -III tubulin and actin signal as follows

$$\text{Tubulin/Actin ratio} = \frac{\beta - \text{III Tubulin intensity}}{\text{Actin intensity}} \quad (1)$$

Over 15 cells were analyzed per image, and 6 images were taken for each condition of 2 independent experiments.

Supporting Information

Supporting Information is available from the Wiley Online Library or from the author.

Acknowledgements

B.D. has received funding by the Spanish ministry of Innovation and Science, Grant PRE2019-088040 funded by MCIN/AEI/10.13039/501100011033 and by "ESF Investing in your future". The University of Trieste, Diputación Foral de Gipuzkoa program Red (101/16), the European Commission (H2020-MSCA-RISE-2016, grant agreement No. 734381, acronym CARBO-IMmap). M.P. as the recipient of the AXA Chair, is grateful to the AXA Research Fund for financial support.

Conflict of Interest

The authors declare no conflict of interest.

Author Contributions

The manuscript was written through contributions from all authors.

Data Availability Statement

The data that support the findings of this study are available in the supplementary material of this article.

Keywords

carbon nanotubes, differentiation, functionalization, neural interfacing, neuroblastoma, tissue engineering

Received: April 21, 2023
Revised: June 29, 2023
Published online:

[1] J. Fertala, M. Rivlin, M. L. Wang, P. K. Beredjiklian, A. Steplewski, A. Fertala, *Brain Behav.* **2020**, *10*, e01802.
[2] *FDA Grants Accelerated Approval for Alzheimer's Disease Treatment | FDA*, https://www.fda.gov/news-events/press-announcements/fda-grants-accelerated-approval-alzheimers-disease-treatment (accessed: February 2023).
[3] Z. Liao, W. Wei, M. Yang, X. Kuang, J. Shi, *Front. Aging Neurosci.* **2021**, *14*, 991140.
[4] E. G. Z. Centeno, H. Cimarosti, A. Bithell, *Mol. Neurodegener.* **2018**, *13*, 27.
[5] J. Li, N. Li, J. Wei, C. Feng, Y. Chen, T. Chen, Z. Ai, X. Zhu, W. Ji, T. Li, *NPJ Parkinsons Dis.* **2022**, *8*, 175.
[6] M. K. Borland, P. A. Trimmer, J. D. Rubinstein, P. M. Keeney, K. Mohanakumar, L. Liu, J. P. Bennett, *Mol. Neurodegener.* **2008**, *3*, 21.
[7] B. Wiatrak, A. Kubis-Kubiak, A. Piwowar, E. Barg, *Cells* **2020**, *9*, 958.
[8] C. Dello Russo, N. Cappoli, I. Coletta, D. Mezzogori, F. Paciello, G. Pozzoli, P. Navarra, A. Battaglia, *J. Neuroinflammation* **2018**, *15*, 259.
[9] Q. Jiao, X. Li, J. An, Z. Zhang, X. Chen, J. Tan, P. Zhang, H. Lu, Y. Liu, *Front. Cell Neurosci.* **2017**, *11*, https://doi.org/10.3389/fncel.2017.00200.
[10] A. E. Pereda, *Nat. Rev. Neurosci.* **2014**, *15*, 250.
[11] C. F. V. Latchoumane, L. Jackson, M. S. E. Sendi, K. F. Tehrani, L. J. Mortensen, S. L. Stice, M. Ghovanloo, L. Karumbaiah, *Sci. Rep.* **2018**, *8*, 10957.
[12] M. Hu, L. Hong, C. Liu, S. Hong, S. He, M. Zhou, G. Huang, Q. Chen, *Sci. Rep.* **2019**, *9*, 4206.
[13] E. W. Keefer, B. R. Botterman, M. I. Romero, A. F. Rossi, G. W. Gross, *Nat. Nanotechnol.* **2008**, *3*, 434.
[14] K. Kim, M.-J. Kim, D. W. Kim, S. Y. Kim, S. Park, C. B. Park, *Nat. Commun.* **2020**, *11*, 2285.
[15] A. Kunisaki, A. Kodama, M. Ishikawa, T. Ueda, M. D. Lima, T. Kondo, N. Adachi, *Sci. Rep.* **2021**, *11*, 19562.
[16] Y. Chemla, E. S. Avraham, A. Markus, E. Teblum, A. Slotky, Y. Kostikov, N. Farah, M. Telkhozhayeva, I. Shoval, G. D. Nessim, Y. Mandel, *Nanoscale* **2020**, *12*, 18918.
[17] H. Wei, Z. Chen, Y. Hu, W. Cao, X. Ma, C. Zhang, X. Gao, X. Qian, Y. Zhao, R. Chai, *Small* **2021**, *17*, 2101017.
[18] V. Lovat, D. Pantarotto, L. Lagostena, B. Cacciari, M. Grandolfo, M. Righi, G. Spalluto, M. Prato, L. Ballerini, *Nano Lett.* **2005**, *5*, 1107.
[19] L. Ye, H. Ji, J. Liu, C.-H. Tu, M. Kappl, K. Koynov, J. Vogt, H.-J. Butt, *Adv. Mater.* **2021**, *33*, 2102981.
[20] A. Dominguez-Alfaro, N. Alegret, B. Arnaiz, M. Salsamendi, D. Mecerreyes, M. Prato, *ACS Appl. Mater. Interfaces* **2020**, *12*, 57330.
[21] H. Mori, Y. Ogura, K. Enomoto, M. Hara, G. Maurstad, B. T. Stokke, S. Kitamura, *PLoS One* **2020**, *15*, e0225589.
[22] J. R. Lee, S. Ryu, S. Kim, B. S. Kim, *Biomater. Res.* **2015**, *19*, 3.
[23] C. Xiang, Y. Zhang, W. Guo, X.-J. Liang, *Acta Pharm. Sin. B* **2020**, *10*, 239.
[24] H. Ravanbakhsh, G. Bao, L. Mongeau, *Sci. Rep.* **2020**, *10*, 2543.
[25] D. Lam, H. A. Enright, J. Cadena, S. K. G. Peters, A. P. Sales, J. J. Osburn, D. A. Soscia, K. S. Kulp, E. K. Wheeler, N. O. Fischer, *Sci. Rep.* **2019**, *9*, 4159.
[26] S. Bosi, A. Fabbro, C. Cantarutti, M. Mihajlovic, L. Ballerini, M. Prato, *Carbon NY* **2016**, *97*, 87.
[27] Y. Sato, A. Yokoyama, Y. Nodasaka, T. Kohgo, K. Motomiya, H. Matsumoto, E. Nakazawa, T. Numata, M. Zhang, M. Yudasaka, H. Hara, R. Araki, O. Tsukamoto, H. Saito, T. Kamino, F. Watari, K. Tohji, *Sci. Rep.* **2013**, *3*, 1911.
[28] B. Joddar, E. Garcia, A. Casas, C. M. Stewart, *Sci. Rep.* **2016**, *6*, 32456.
[29] P. C. B. D.e Faria, L. I. D. Santos, J. P. Coelho, H. B. Ribeiro, M. A. Pimenta, L. O. Ladeira, D. A. Gomes, C. A. Furtado, R. T. Gazzinelli, *Nano Lett.* **2014**, *14*, 5458.
[30] H. Shao, T. Li, R. Zhu, X. Xu, J. Yu, S. Chen, L.i Song, S. Ramakrishna, Z. Lei, Y. Ruan, L. He, *Biomaterials* **2018**, *175*, 93.
[31] H. Hu, Y. Ni, V. Montana, R. C. Haddon, V. Parpura, *Nano Lett.* **2004**, *4*, 507.
[32] V. Mathur, S. Talapatra, S. Kar, Z. Hennighausen, *ACS Appl. Bio Mater.* **2021**, *4*, 4071.
[33] S. Usmani, A. F. Biagioni, M. Medelin, D. Scaini, R. Casani, E. R. Aurand, D. Padro, A. Egimendia, P. R. Cabrer, M. Scarselli, M. De Crescenzi, M. Prato, L. Ballerini, *Proc. Natl. Acad. Sci. USA* **2020**, *117*, 25212.
[34] X. Hu, X. Wang, Y. Xu, L. Li, J. Liu, Y. He, Y. Zou, L. Yu, X. Qiu, J. Guo, *Adv. Healthcare Mater.* **2020**, *9*, 1901570.
[35] W. Pi, L. Zhou, W. Zhang, S. Liu, C. Li, M. Zhang, Y. Wen, P. Zhang, *J. Mater. Sci.* **2022**, *57*, 11289.
[36] A. Kolanowska, P. Wasik, W. Zieba, A. P. Terzyk, S. Boncel, *RSC Adv.* **2019**, *9*, 37608.
[37] J. L. Bahr, J. M. Tour, *Chem. Mater.* **2001**, *13*, 3823.
[38] J. M. González-Domínguez, A. Santidrián, A. Criado, C. Hadad, M. Kalbáč, T. da Ros, *Chemistry* **2015**, *21*, 18631.
[39] B. R. C. de Menezes, F. V. Ferreira, B. C. Silva, E. A. N. Simonetti, T. M. Bastos, L. S. Cividanes, G. P. Thim, *J. Mater. Sci.* **2018**, *53*, 14311.
[40] M. M. Kaid, A. Gebreil, S. A. El-Hakam, A. I. Ahmed, A. A. Ibrahim, *RSC Adv.* **2020**, *10*, 15586.
[41] R. A. Ando, G. M. D. Nascimento, R. Landers, P. S. Santos, *Spectrochim. Acta, Part A* **2008**, *69*, 319.
[42] C.-W. Huang, H. Teng, *J. Electrochem. Soc.* **2008**, *155*, A739.
[43] S. Oh, M. Jang, J. Kim, J. Lee, H. Zhou, J. Lee, *Curr. Appl. Phys.* **2016**, *16*, 738.
[44] S. Yang, J. Huo, H. Song, X. Chen, *Electrochim. Acta* **2008**, *53*, 2238.
[45] Y. Zhang, K. Li, P. Ji, D. Chen, J. Zeng, Y. Sun, P. Zhang, J. Zhao, *J. Mater. Sci.* **2017**, *52*, 3630.
[46] C.-T. Hsieh, W.-Y. Chen, Y.-S. Cheng, *Electrochim. Acta* **2010**, *55*, 5294.
[47] H. Hu, Y. Ni, V. Montana, R. C. Haddon, V. Parpura, *Nano Lett.* **2004**, *4*, 507.